The Influence of the Andes Cordillera on Transient Disturbances

MANOEL ALONSO GAN AND VADLAMUDI BRAHMANANDA RAO

Instituto Nacional de Pesquisas Espaciais—Inpe São José Dos Campos, São Paulo, Brazil

(Manuscript received 12 October 1992, in final form 22 October 1993)

ABSTRACT

The influence of the Andes Cordillera on transient disturbances is investigated in this study using a lag-correlation analysis. This analysis shows that the unfiltered geopotential height data have a wavelike pattern moving to the east while tilting to the west in the vertical. When the wave approaches the Andes Cordillera, it exhibits orographic effects such as anticyclonic turning of a low-level disturbance trajectory, a zonal trajectory in the upper levels, distortions of the isolines of correlation, and an elongation of maximum correlation on the lee side of the Andes. The anticyclonic turning of the trajectory in the low-altitude levels and a zonal trajectory in upper levels implies a decrease in the vertical tilt of the system on the windward side and an increase in the tilt on the lee side. The increase of baroclinicity on the lee side results in baroclinic development as predicted from a linearly obtained normal-mode solution in the presence of mountains.

A cross-correlation analysis of the high-pass-filtered disturbances shows an eastward phase propagation and a westward vertical tilt with height on the order of one-quarter wavelength between 1000- and 300-hPa levels. The horizontal structure and phase propagation show characteristics similar to the fastest-growing baroclinic normal mode in a two-layer, quasigeostrophic, β-plane, linear model with a mountain placed in the north–south direction. This shows that the high-pass-filtered anomalies over the South American region are associated with baroclinic disturbances influenced by the Andes Cordillera. The results further show that the interaction of these anomalies with the Andes Cordillera is responsible for lee cyclogenesis. The composite maps show that the positive and negative high-pass-filtered anomalies have the same structure and paths of phase propagation. These anomalies intensify over the Pacific Ocean near the South American continent.

1. Introduction

The influence of mountains on the general circulation of the atmosphere, in the generation of mountain–valley breezes and in lee cyclogenesis has been the subject of several studies (WMO 1980). In the Northern Hemisphere most of the large mountain ranges are located in the midlatitudes, blocking the westerly winds and the transient disturbances embedded in them. Although a large part of the Andes Cordillera (hereafter called the Andes) is located in the tropics, it affects the atmospheric circulations of the southern part of South America. The effect of the Andes was studied by Satyamurty et al. (1980) using a numerical model. Satyamurty et al. showed the formation of a stationary trough on the lee side of the Andes. The influence of the Andes on the transient disturbances did not receive much attention. Nevertheless, synoptic experience shows that cold fronts and low pressure systems become weakened as they approach the Andes and intensify on the lee side of the Andes.

The subject of cyclogenesis on the lee side of a mountain, particularly in the region of the Alps, has been extensively studied (Buzzi et al. 1987; Pichler and Steinacker 1987; McGinley and Zupanski 1990; and many others). Although the geometry of the Rockies is different from that of the Alps, some common features of lee cyclogenesis have been observed. One such feature is the existence of a low pressure system that dissipates as it crosses the mountain and generates another cyclone farther south on the lee side. Another important aspect in the initiation of the lee cyclone is the interaction of topography with the cold front associated with the preexisting cyclone due to the reduction of cold-air advection on the lee side, distortion of the frontal structure, and the appearance of positive thermal anomalies on the lee side (Buzzi and Tibaldi 1978). At this stage a thermally direct circulation is generated, converting eddy available potential energy into eddy kinetic energy, indicating that the development of lee cyclones has a strong baroclinic component (McGinley 1982).

One of the earliest studies aimed at understanding the effects of mountains in the formation of cyclones was due to Egger (1972). In this study he used a primitive equation model, and the mountain was represented by a vertical wall. The results of Egger (1972, 1974) showed the importance of mean baroclinic flow and the direct interaction of a preexisting low with topography. However, the theoretical model of cyclogenesis devel-

Corresponding author address: Dr. Manoel Alonso Gan, CPTEC, INPE, C.P. 515, 12201 São José dos Campos, São Paulo, Brazil.

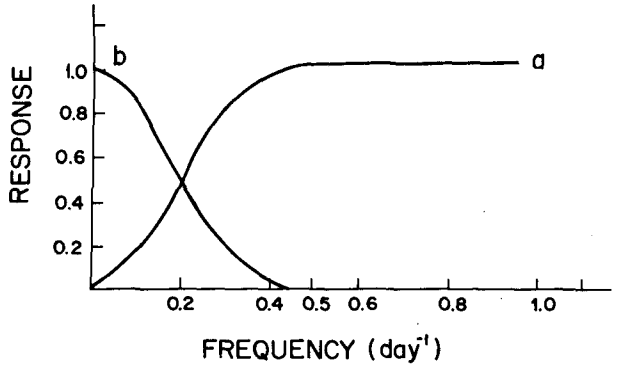

FIG. 1. Frequency response of (a) the high-pass filter and (b) the low-pass filter.

oped by Speranza et al. (1985) shows, in contrast to that of Egger, that the formation of lee cyclones is related to the rising and sinking motion associated with baroclinic waves, not with the mean current.

Hayes et al. (1987) proposed that lee cyclogenesis is a result of the superposition of a stationary wave generated by the mountain and a transient baroclinic disturbance. Mean flow over a mountain range of synoptic scale generates a high pressure ridge over the mountain and a trough of low pressure on the lee side (Eliassen and Palm 1961; Satyamurty et al. 1980). Thus, a transient cyclonic disturbance is partially canceled as it approaches the ridge. On the lee side, however, intensification of the transient disturbance is observed because of the superposition of the transient cyclone on the mountain trough. Thus, on the lee side of a mountain, intensification might appear as the gener-

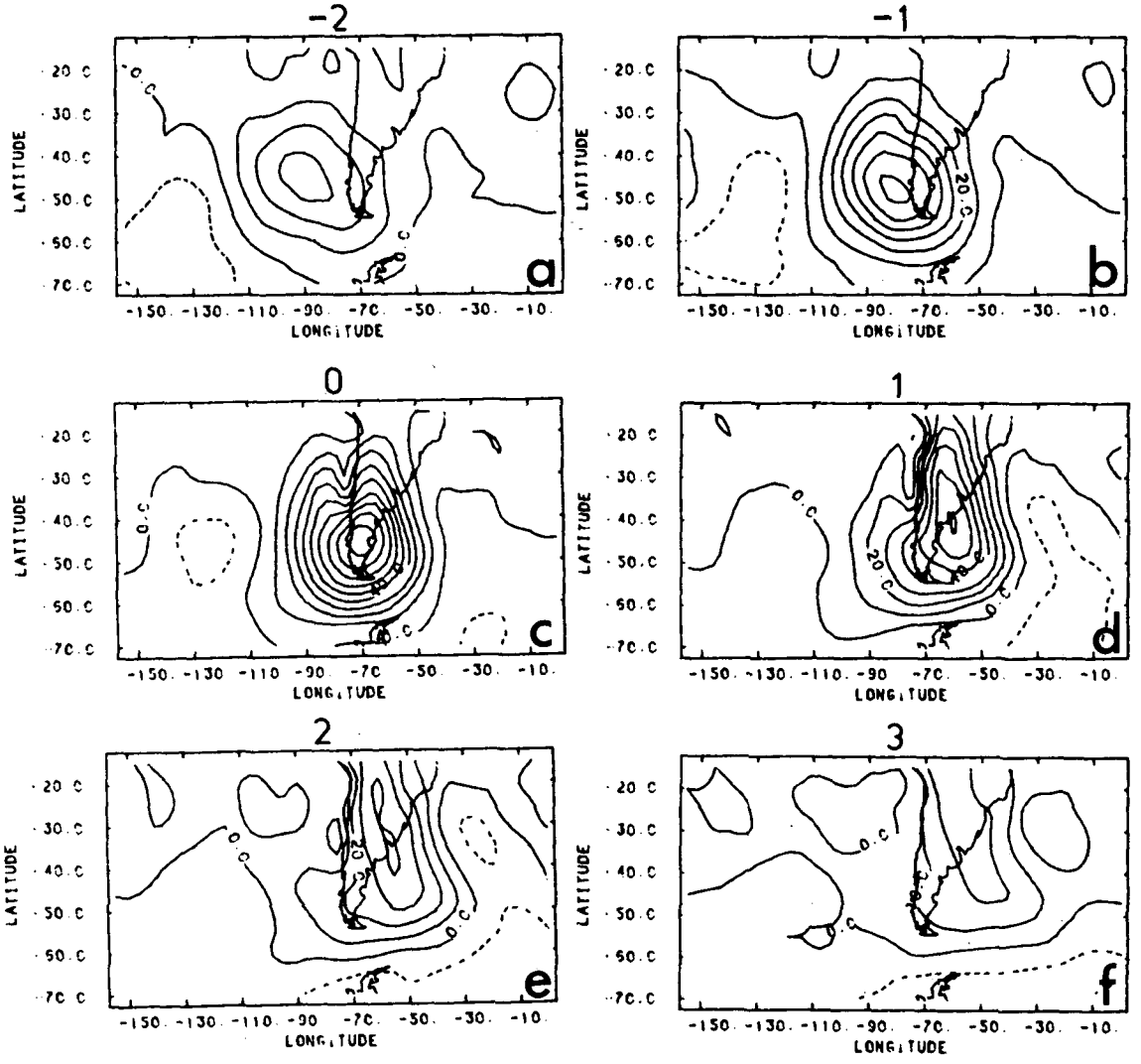

FIG. 2. Correlation coefficient (%) between unfiltered geopotential height of 1000 hPa at 45°S, 70°W and unfiltered geopotential height of 1000 hPa at every grid point: (a) 2 days earlier, (b) 1 day earlier, (c) at the same time, (d) 1 day later, (e) 2 days later, and (f) 3 days later. The contour interval is 10%; negative contours are dashed.

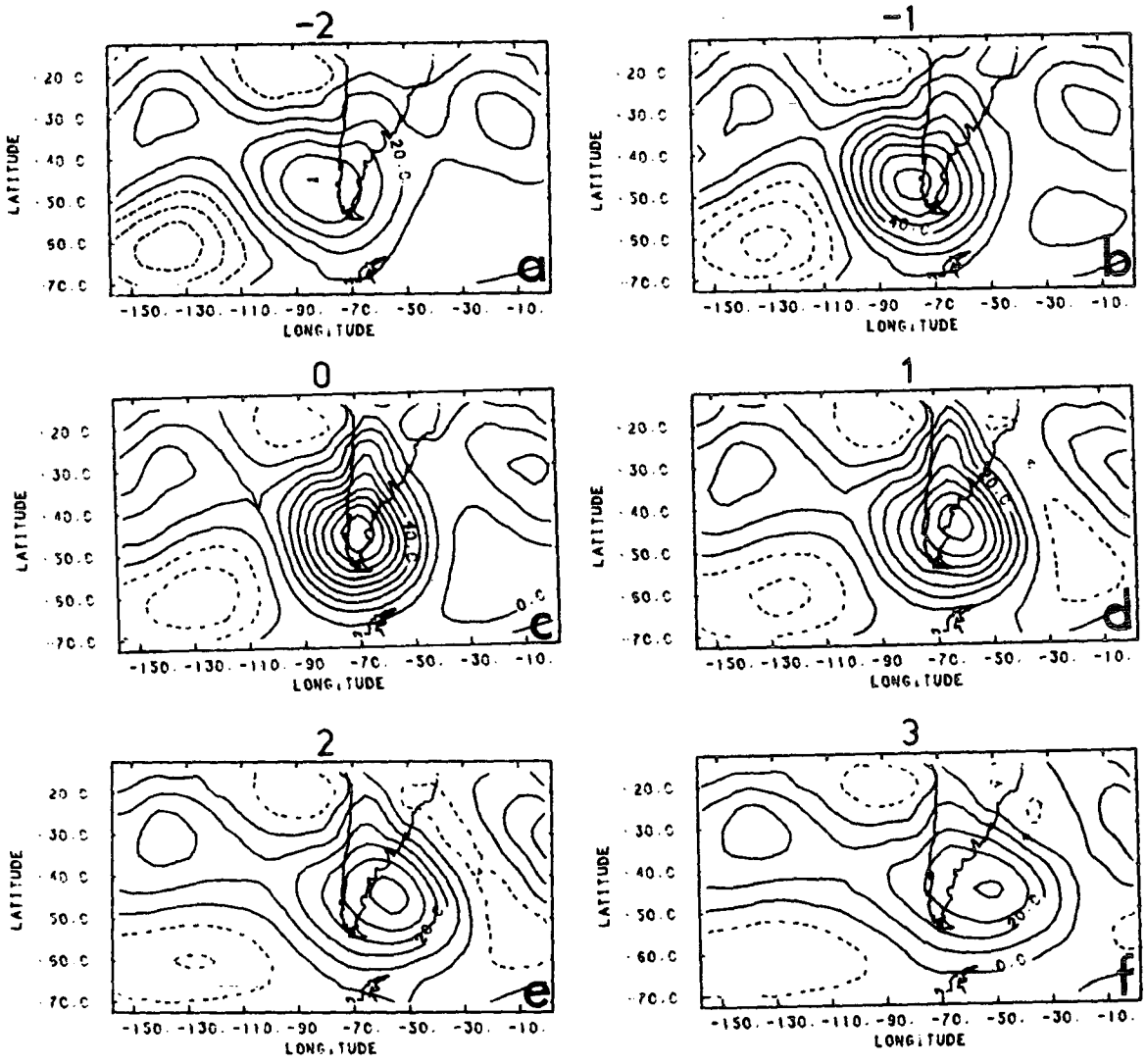

FIG. 3. Correlation coefficient (%) between unfiltered geopotential height of 700 hPa at 45°S, 70°W and unfiltered geopotential height of 700 hPa at every grid point: (a) 2 days earlier, (b) 1 day earlier, (c) at the same time, (d) 1 day later, (e) 2 days later, and (f) 3 days later. The contour interval is 10%; negative contours are dashed.

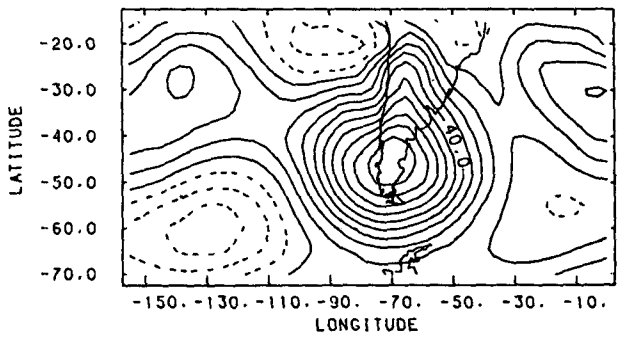

FIG. 4. Correlation coefficient (%) between low-pass-filtered geopotential height of 700 hPa at 45°S, 70°W and low-pass-filtered geopotential height of 700 hPa at every grid point at the same time. The contour interval is 10%; negative contours are dashed.

ation of a surface cyclone. This theory of Hayes et al. (1987) seems to apply to the development of cyclones over the central region of South America, since a disturbance coming from the Pacific many times seems to intensify as it moves into the lee side of the Andes and generates a surface cyclone.

On the other hand, Buzzi and Tossi (1989) and Buzzi et al. (1990) suggested that lee cyclogenesis is the effect of the interaction of high-frequency disturbances with a mountain. Calculating the fields of autocorrelation coefficients of high-pass-filtered geopotential height data obtained from a quasigeostrophic model, Buzzi et al. (1990) showed that the high-frequency disturbances passing over the Alps or the Rockies possess structures very similar to those of normal

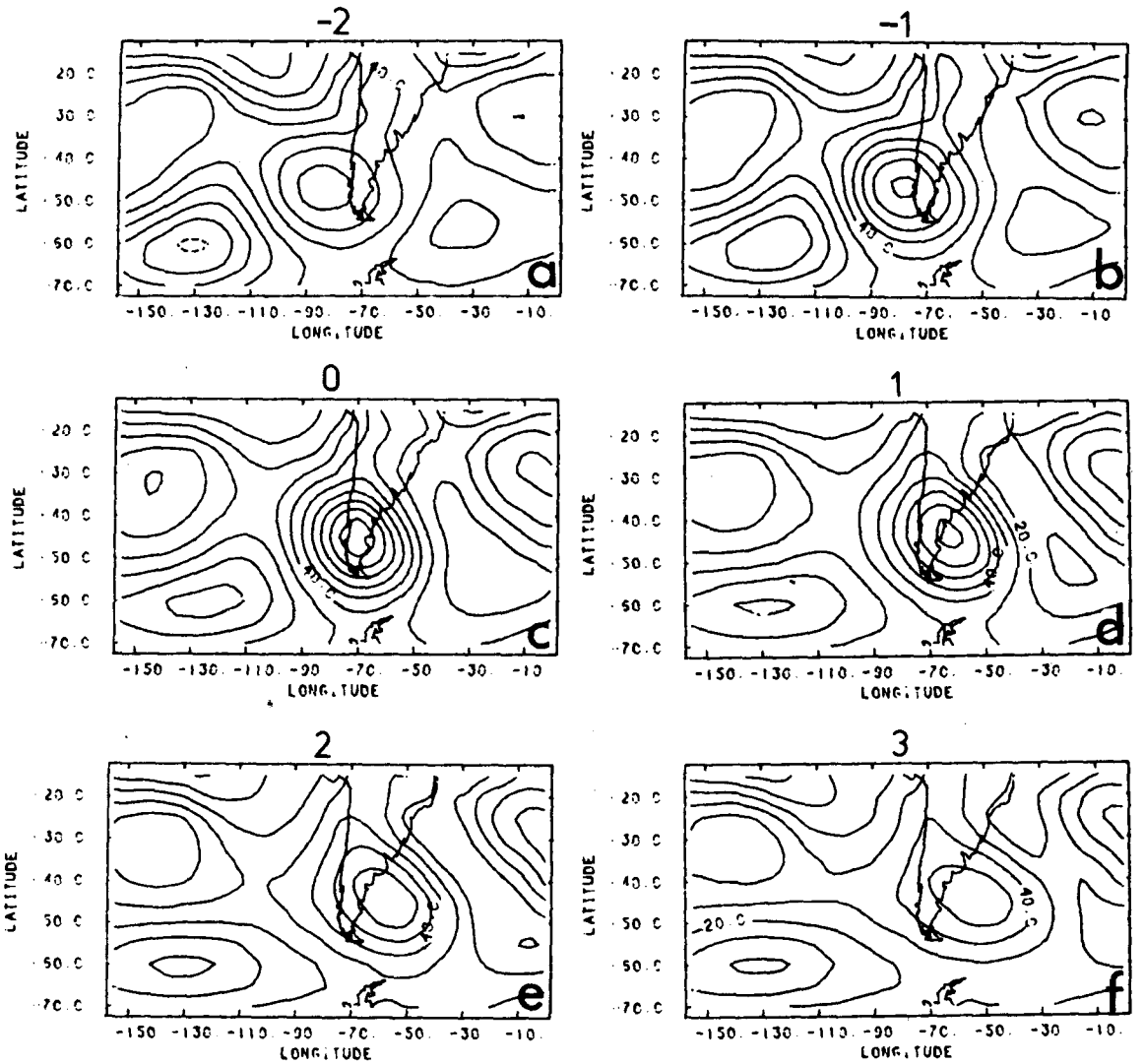

FIG. 5. Correlation coefficient (%) between unfiltered geopotential height of 300 hPa at 45°S, 70°W and unfiltered geopotential height of 300 hPa at every grid point: (a) 2 days earlier, (b) 1 day earlier, (c) at the same time, (d) 1 day later, (e) 2 days later, and (f) 3 days later. The contour interval is 10%; negative contours are dashed.

modes of the most unstable disturbances obtained by Buzzi et al. (1987) in a linear quasigeostrophic model with a mountain. Further, Buzzi et al. (1990) compared the results of statistical analysis with the horizontal structures of normal modes of baroclinic waves. They found a similarity in characteristics such as the existence of a maximum standard deviation on the lee side, a minimum standard deviation on the upwind side, and a dipole in the fields of correlation between high and low levels.

Hsu (1987) showed that the influence of orography in the unfiltered data is such that the vertical structure of the disturbances is equivalent barotropic on the west side of the mountain, while on the east side it is baroclinic. This effect is due to the displacement of the disturbances parallel to the mountains in the lower levels provoked by the generation of a topographic Rossby wave (Wallace 1986). These topographic Rossby waves considered by Hsu (1987), which propagate along topographic slopes that effectively act as β planes, are different from stationary planetary waves (also called topographic Rossby waves) forced by topography on a β plane. Hsu also noted that the patterns of correlation for the unfiltered data show a quasi-stationary bipolar structure on the west of the Rockies, and on the east there is development of another center of correlation. This development is interpreted by Hsu as the dispersion of stationary wave energy in two dimensions. High-frequency disturbances possess a weak westward inclination with height on the west side of

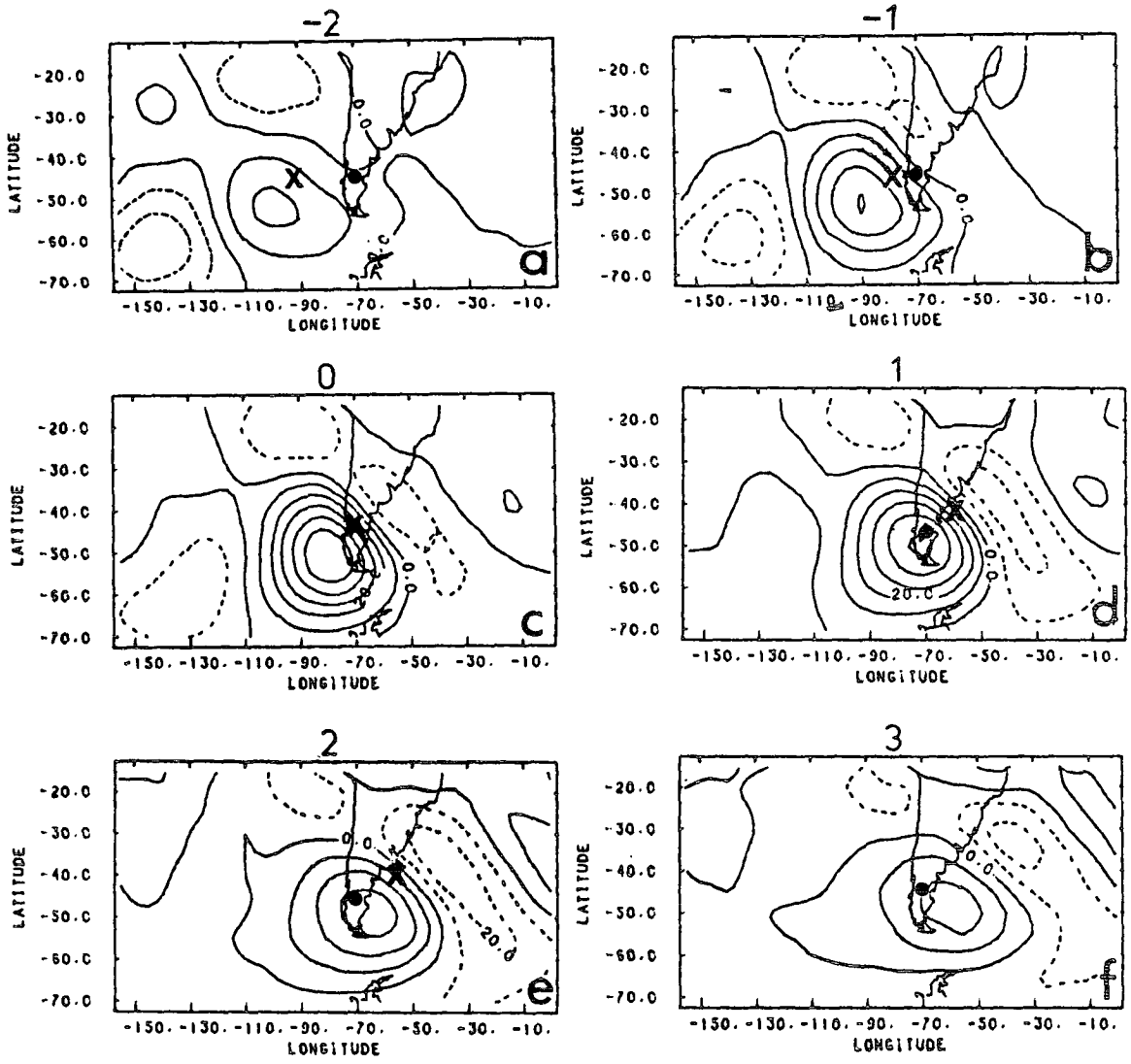

FIG. 6. Correlation coefficient (%) between unfiltered geopotential height of 1000 hPa at 45°S, 70°W (indicated by a dot) and unfiltered geopotential height of 300 hPa at every grid point: (a) 2 days earlier, (b) 1 day earlier, (c) at the same time, (d) 1 day later, (e) 2 days later, and (f) 3 days later. Contour interval 10%; negative contours are dashed. The "X" represents the position of the respective minimum or maximum center at 1000 hPa.

Rockies and a strong westward inclination with height on the east side. The effect of mountains is also noted on the trajectory of the high-frequency disturbances. The trajectory is anticyclonic in the lower levels and at 500 hPa it is parallel to the mean flow at 700 hPa. This feature is evidence of Rossby waves being generated by the topography, since in the lower levels the movement is not parallel to the mean flow of the midtroposphere. In the region of the Tibetan Plateau, Hsu observed that the high-frequency disturbances close to the mountains showed some characteristics of Kelvin waves such as the small lateral scale and high velocity of propagation.

The purpose of the present study is to determine how the Andes affect transient disturbances and if there is any evidence of orographically induced waves. The method employed is similar to that used earlier by Buzzi and Tosi (1989) and Hsu (1987). We propose to use cross-correlational analysis of unfiltered and high-pass-filtered geopotential height data. The results obtained in this study will be compared with the existing theory of orographic flow modification. As far as we know this type of study has not yet been performed for this region.

2. Data and methodology

In this study we used geopotential height data for 1000, 700, and 300 hPa for the period 1 January 1977–31 December 1979. These are the twice-daily analyses

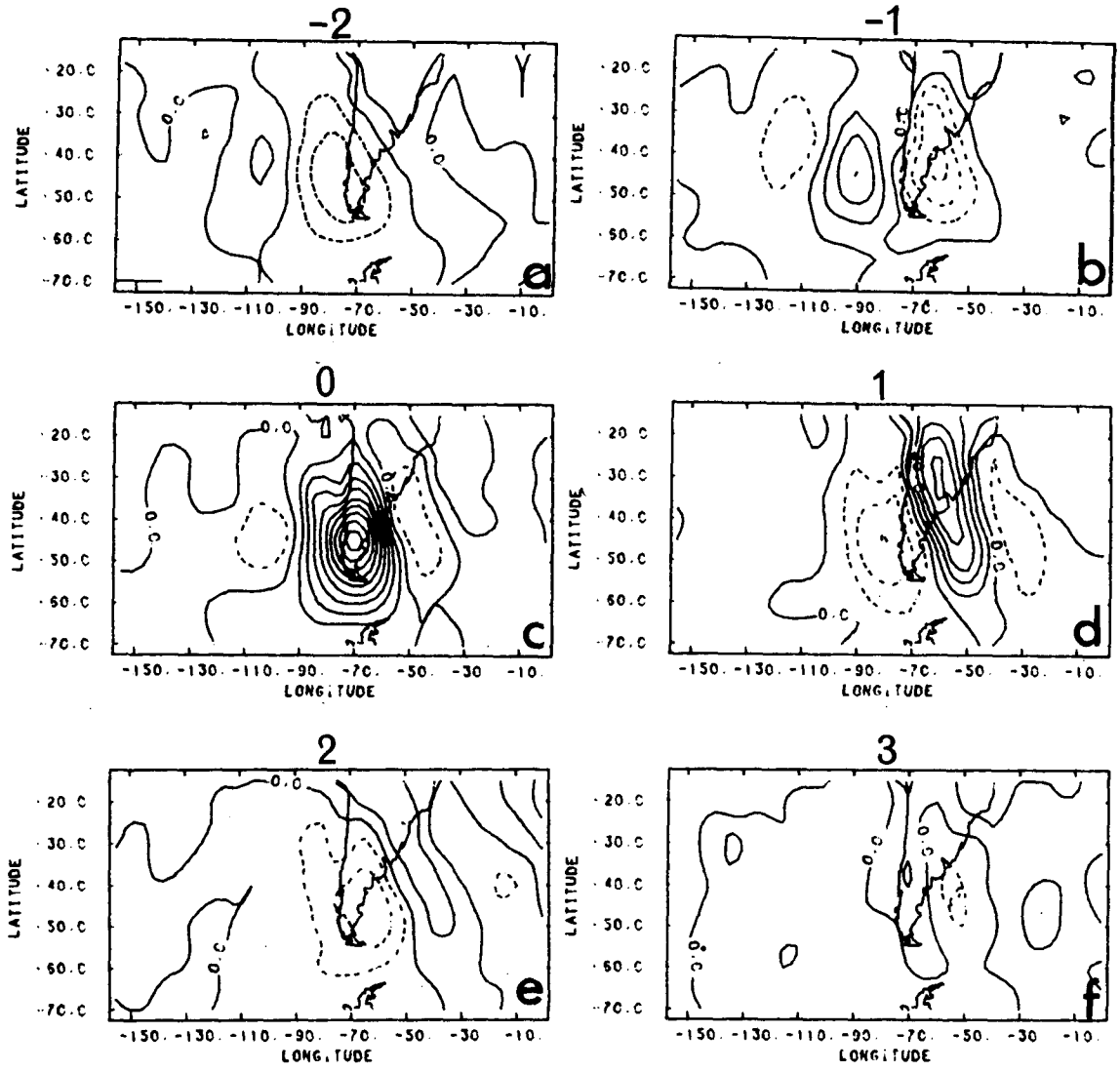

FIG. 7. Correlation coefficient (%) between high-pass-filtered geopotential height of 1000 hPa at 45°S, 70°W and high-pass-filtered geopotential height of 1000 hPa at every grid point: (a) 2 days earlier, (b) 1 day earlier, (c) at the same time, (d) 1 day later, (e) 2 days later, and (f) 3 days later. The contour interval is 10%; negative contours are dashed.

provided by the National Meteorological Center (NMC) and are on a 2.5° × 2.5° latitude–longitude grid. However, because of the short memory of the computer on hand, only 5° × 5° gridpoint data were used. Data were missing for the period of 16 June 1977–31 July 1977. Other missing 1-day data were linearly interpolated.

In the present analysis no attempt is made to separate the data by season, since we feel that seasonal differences are not substantial in the Southern Hemisphere (Palmén and Newton 1969), and as Randel and Stanford (1985a,b,c) have shown that transient baroclinic disturbances occur in the Southern Hemisphere during summer also. We made use of unfiltered and high-pass-filtered data with periods shorter than 5 days. The filter used is of a Gaussian type with nine points in the time series and is given by (1) and (2). This filter is essentially the same as that used earlier by Lau and Lau (1984) and Hsu (1987):

$$X_l(t) = \sum_{m=-4}^{4} a_m X(t-m) \qquad (1)$$

$$X_h(t) = X(t) - X_l(t), \qquad (2)$$

where $a_0 = 0.2041636$, $a_{-1} = a_1 = 0.1801738$, $a_{-2} = a_2 = 0.1238316$, $a_{-3} = a_3 = 0.0662822$, and $a_{-4} = a_4 = 0.0276306$.

Initially, X_l time series were determined by removing all fluctuations with periods shorter than 5 days. Then these series were subtracted from the original series to

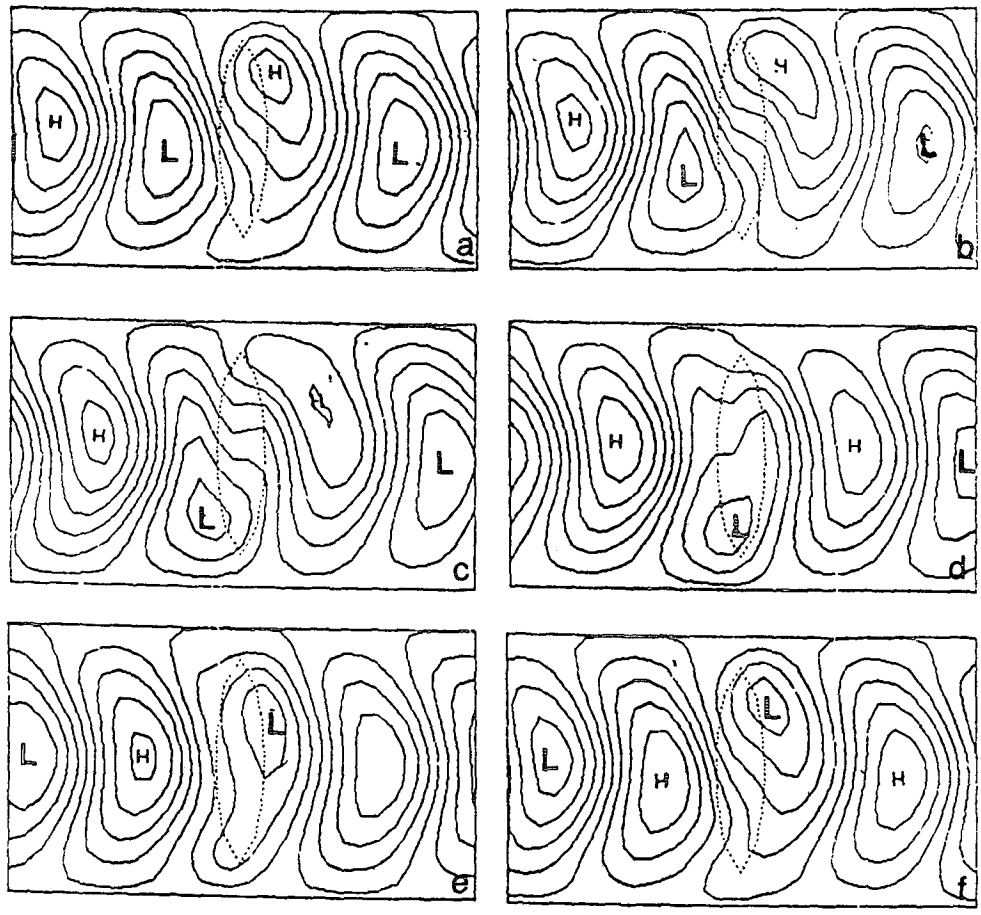

FIG. 8. The structure and evolution during an entire cycle of the most unstable normal mode (streamfunction) in the lower layer of a two-layer channel model, oriented from west to east (β plane). Channel length and width are 10 000 and 6000 km, respectively. The basic-state mean velocity is 17 m s^{-1} in the upper layer and 0 m s^{-1} in the lower; a sheared component of velocity in the upper layer is added with a profile $\cos[\pi(2y/L_y - 1)]$ and amplitude of 4 m s^{-1}. The mountain range is bi-Gaussian, with maximum height H_{max} = 2500 m. The H_{max}/e contour is dotted. The six maps are for different times of evolution of the baroclinic mode but with the same amplitude normalization. The figure is adapted for the Southern Hemisphere. Source: Buzzi et al. (1987).

obtain the high-pass-filtered data. The frequency response of the operations is shown in Fig. 1. The purpose of the usage of this filter is to study the behavior of high-frequency transient disturbances as they approach the Andes. Correlation maps and the composite maps were also prepared. The correlations were calculated using the equation

$$R_n = \frac{\Sigma_t[y(t) - \bar{y}][X_n(t + \Delta t) - \bar{X}]}{\{\Sigma_t[y(t) - \bar{y}]^2\Sigma_t[X_n(t + \Delta t) - \bar{X}]^2\}^{1/2}}$$

$$\text{for } n = 1, 2 \ldots . ij, \quad (3)$$

where j is the number of latitude points and i is the number of longitude points, $y(t)$ is the time series of a base grid point, $X(t + \Delta t)$ is the time series with a time lag, and Δt is the time lag with a 12-h interval. Grid points near the Andes were selected as the base grid points for computing lag correlations and for compositing. Through this analysis the structure and evolution of the disturbances can be determined.

3. Results

Recent studies by Wallace et al. (1988), Hsu (1987), and others have shown that the fields of lagged correlations can furnish important details regarding the evolution and structure of high- and low-frequency disturbances, particularly the effect of mountains on the low-level circulation. Thus, a base grid point over the continent (45°S, 70°W) was selected to calculate the fields of correlations.

Figure 2 shows the map of correlation coefficients between the unfiltered geopotential height at 1000 hPa at the base grid point 45°S, 70°W and geopotential height at all the other grid points at the same level. It

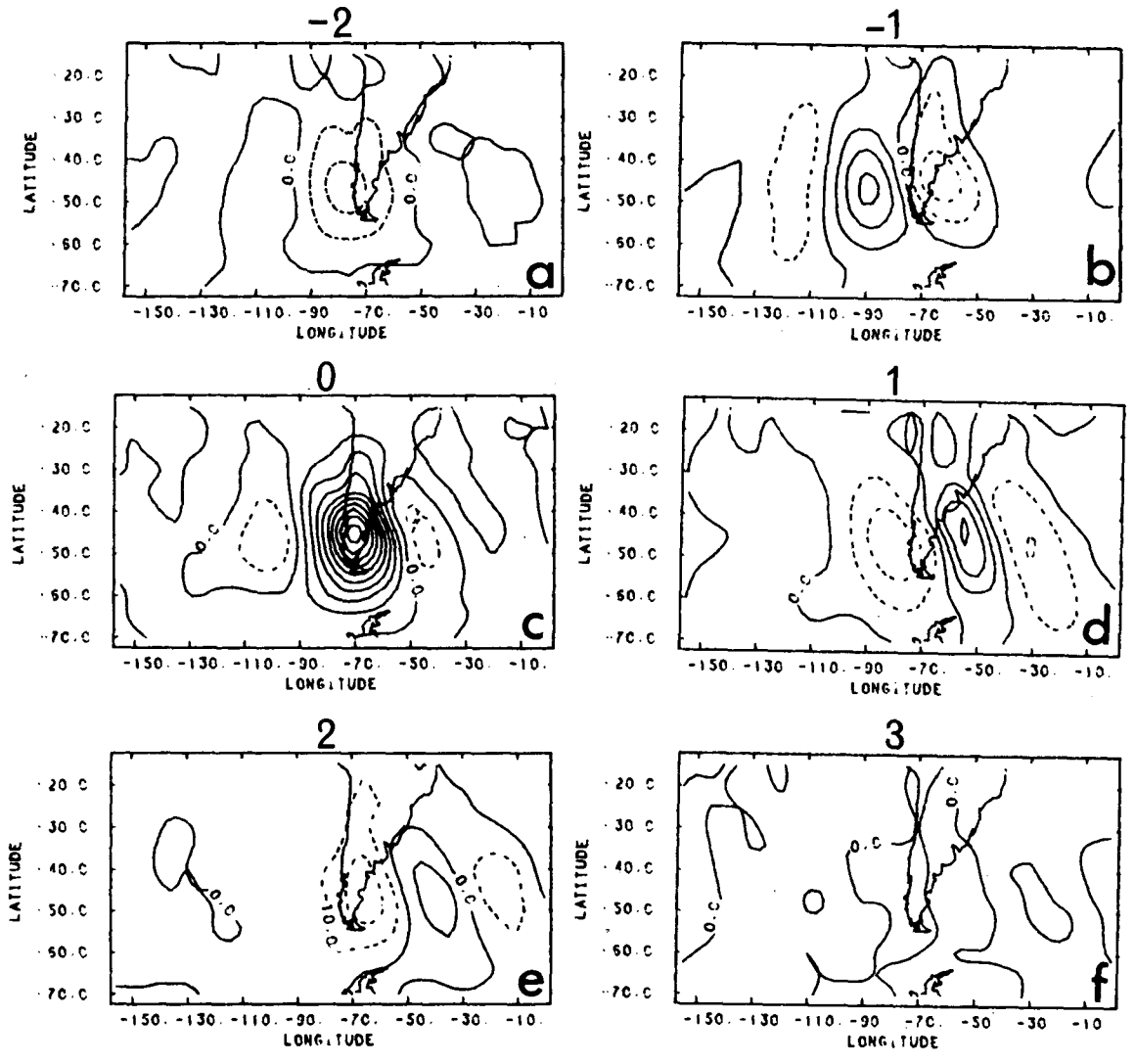

FIG. 9. Correlation coefficient (%) between high-pass-filtered geopotential height of 700 hPa at 45°S, 70°W and high-pass-filtered geopotential height of 700 hPa at every grid point: (a) 2 days earlier, (b) 1 day earlier, (c) at the same time, (d) 1 day later, (e) 2 days later, and (f) 3 days later. The contour interval is 10%; negative contours are dashed.

can be seen in this figure that there is a wave pattern on day 0, which propagates to the east with a phase velocity of about 10° of longitude per day. This pattern has a wavelength of about 95° of longitude and a meridional scale of 50° of latitude. Phase velocity is calculated taking the movement of center of maximum correlation between day −1 and day +1 and dividing by 2. From day −1 through day +2 distortions are seen in the isolines of maximum correlation on the west side of the Andes, which can be attributed to mountain and coastal effects. However, since these distortions are seen only on the west coast and not on the east coast, they are more due to the mountain effect than to the coastal effect. On day 0 (Fig. 2c), the center of maximum correlation is extended to north and central Argentina. In the same map the distortions in the isolines of correlations possess a wave form reminiscent of the dipole structure obtained by Speranza et al. (1985) for the Alps. On day +1 (Fig. 2d) the gradient in the isolines of correlation increases over the Andes, and on day +2 (Fig. 2e) two centers of maximum correlation are observed over the continent. Another interesting aspect in this evolution is the increase in the meridional scale of the center of maximum correlation on the lee side of the Andes. As mentioned in the introduction, this result was also observed on the lee side of the Rockies by Hsu (1987) (see Fig. 2 of Hsu 1987). According to Hsu, this elongation happens because of two different types of behavior: 1) the more stationary dipolelike feature with an equivalent barotropic vertical structure to the west of the Rockies does not move much during the sequence, and 2) a more baroclinic

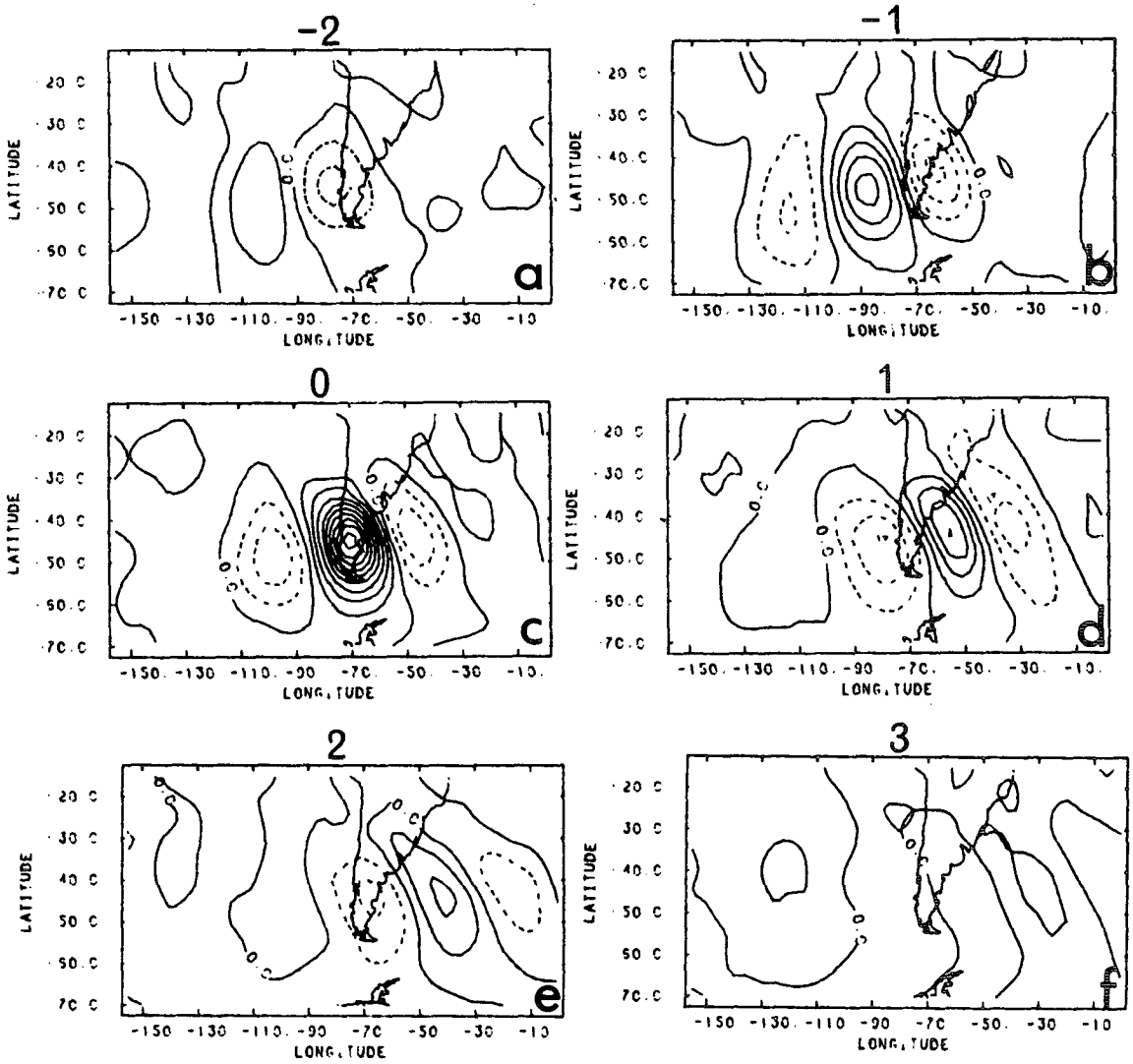

FIG. 10. Correlation coefficient (%) between high-pass-filtered geopotential height of 300 hPa at 45°S, 70°W and high-pass-filtered geopotential height of 300 hPa at every grid point: (a) 2 days earlier, (b) 1 day earlier, (c) at the same time, (d) 1 day later, (e) 2 days later, and (f) 3 days later. The contour interval is 10%; negative contours are dashed.

vertical structure along the eastern slopes of the Rockies shows a clear phase propagation. This is an indication of the superposition of transient baroclinic disturbances upon the stationary Rossby wave generated by the mountain (Hayes et al. 1987).

Figure 3 is similar to the previous figure except that it is for 700 hPa. At this level the effect of the Andes is still present in the distortions of the isolines of correlation and in the elongation of maximum correlation on the lee side of the Andes. These effects remained throughout the evolution. The zonal and meridional scales of the wave are the same as noted earlier for 1000 hPa, although the phase speed is a little less (7.5° of longitude per day). In Fig. 3, other centers also can be seen, and the centers located over the Pacific Ocean remain stationary. This pattern is similar to that shown in Fig. 4, which is for the low-pass disturbances for day 0. Thus, the unfiltered data represent better the behavior of low-frequency systems. Since the wave generated by the mountains depends on the direction of wind that impinges on the mountains, the quasi-stationary (low-frequency) flux possesses a more predominant direction than the high-frequency flux for the formation of a lee wave.

Figure 5 is constructed in the same way as Fig. 2 but for 300 hPa. The phase velocity and zonal wavelength are of the same order of magnitude as those found at 700 hPa. The meridional scale, however, is somewhat smaller (about 30° of latitude). The centers of maximum and minimum correlation over the Pacific Ocean also remain stationary. The wave pattern at this level is similar to that noted for 700 hPa but does not show

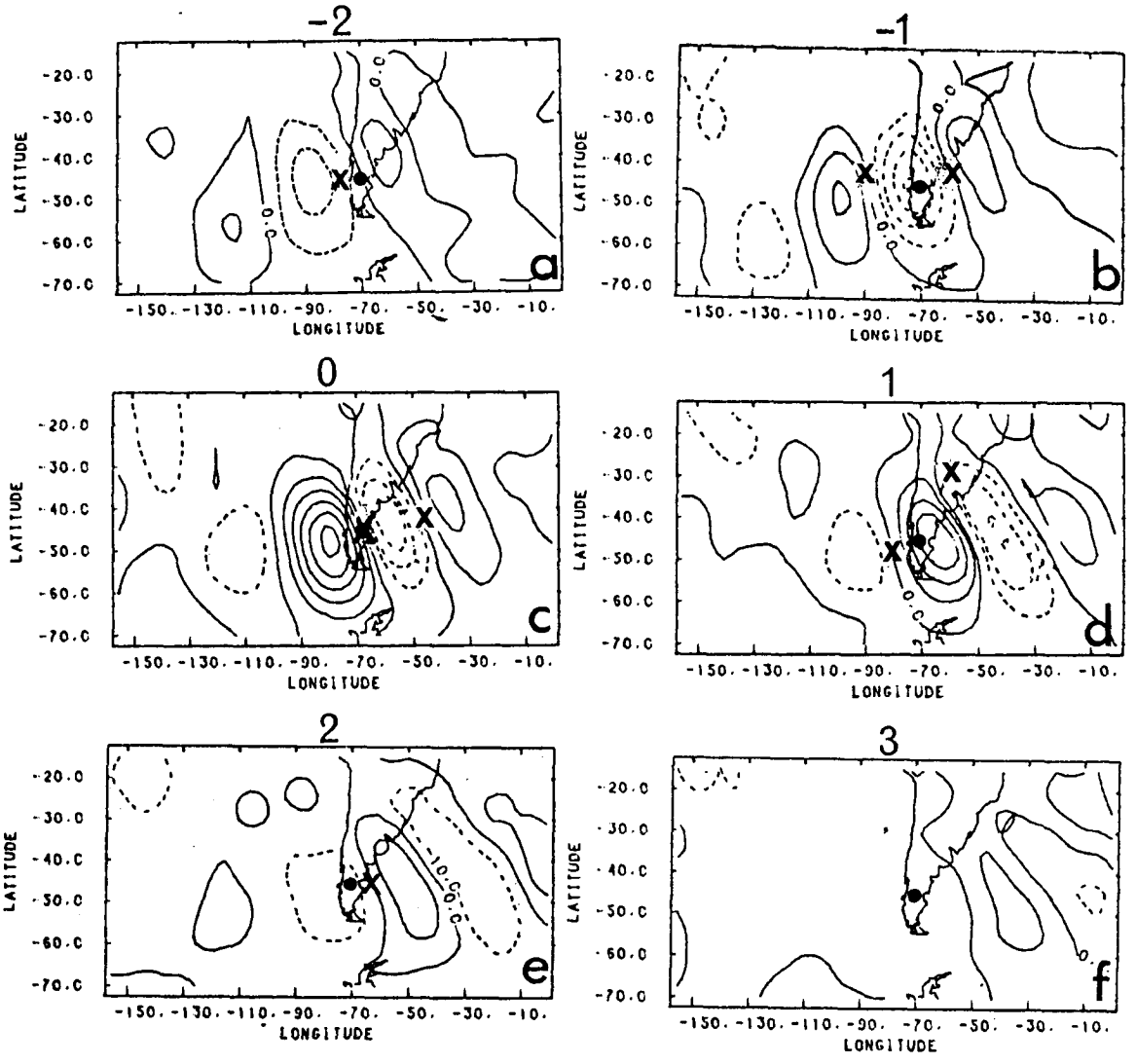

FIG. 11. Correlation coefficient (%) between high-pass-filtered geopotential height of 1000 hPa at 45°S, 70°W (indicated by a dot) and high-pass-filtered geopotential height of 300 hPa at every grid point: (a) 2 days earlier, (b) 1 day earlier, (c) at the same time, (d) 1 day later, (e) 2 days later, and (f) 3 days later. The contour interval is 10%; negative contours are dashed. The "X" represents the respective minimum or maximum center at 1000 hPa.

distortions associated with the mountains effects in the isolines of the center of maximum correlation. A careful examination of Figs. 3 and 5 (for +1 day) shows a slight inclination to the west of the elongation between 700 and 300 hPa.

Maps of correlation between the time series of the base grid point at 1000 hPa and the geopotential height data at 300 hPa provide information regarding the vertical structure of the disturbance. Figure 6 shows these maps for the base grid point 45°S, 70°W. Comparing the positions of centers of maximum correlation in Fig. 6 with those in Fig. 2, one can note that the disturbances exhibit a slight inclination to the west with height over the Pacific Ocean. The inclination increases as the disturbances move over South America. Also we can see in this figure that on day 0 a center of negative correlation appears on the downwind side of the center of maximum correlation. A similar situation was also observed by Hsu (1987) for the Rocky Mountains, and Hsu interpreted this as the result of the dispersion of Rossby wave energy.

Since the unfiltered data represent the low-frequency system, it is necessary to use a high-pass filter to verify the influence of the Andes on the propagation of transient disturbances of high frequency. Thus, Figs. 7, 9, 10, and 11 are similar to Figs. 2, 3, 5, and 6, respectively, except that the former ones are for high-pass-filtered data. The purpose of repeating the analysis with filtered data is to see the horizontal and vertical structure of high-pass disturbances and their interaction with

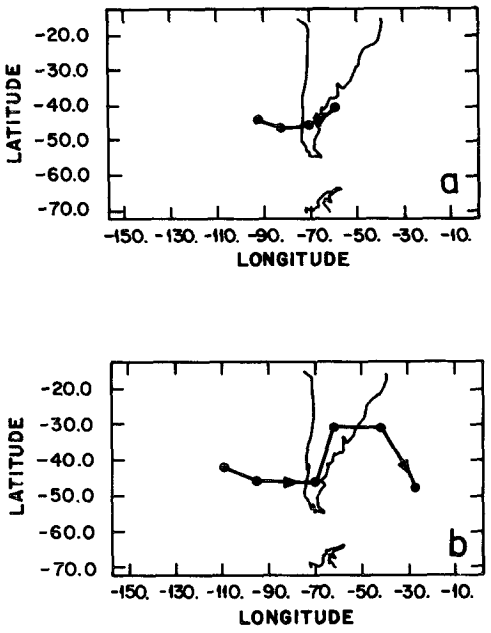

FIG. 12. Trajectory of the center of maximum correlation at 1000 hPa: (a) unfiltered and (b) high-pass-filtered geopotential height data. Temporal separation of the points is 24 h.

the Andes. In Fig. 7 one can see that the wave pattern is better defined in the filtered data. The zonal wavelength on day 0 is 60° of longitude (wavenumber 6) and is smaller than that seen for unfiltered data. This figure also shows distortions in the isolines of correlations and elongation of the centers of maximum and minimum correlation. It can also be seen that from day 0 to day +1 there is a displacement of the center of maximum correlation toward the north.

The observed characteristics of the wave patterns in Fig. 7 such as the distortions of the isolines of correlation and the sudden change in the position of the center of maximum correlation are very similar to the structures of the normal modes obtained from the quasigeostrophic theory of lee cyclogenesis proposed by Buzzi et al. (1987). Figure 8 shows the structure and evolution of the fastest-growing baroclinic mode due to the baroclinic instability of a zonal current in the presence of a meridionally oriented mountain with a maximum height of 2500 m. In this figure the characteristics of the wave patterns such as the distortion and sudden change in the position of the low pressure center can be seen. However, there is one important difference. The intensity of the highs and lows is the same in the normal-mode solution. In the centers of maximum and minimum correlation the intensity is different. This difference exists because the model of Buzzi et al. (1987) is linear while the atmosphere is highly nonlinear. In addition, asymmetry of terrain, land–ocean contrast, and analysis or model errors might also play some role.

Buzzi and Tosi (1989) and Buzzi et al. (1990) also noted a wave pattern in the high-frequency anomalies near the Rockies although the criterion for selection of data in Buzzi and Tosi (1989) favored lee cyclogenesis, and Buzzi et al. (1990) used the data derived from a simulation with a quasigeostrophic model with topography. In Hsu (1987), who used time series data for 21 winters, the sudden change in the position of the centers of correlations as noted in the normal modes of baroclinic waves in the presence of a mountain was not observed. This difference could be a result of how the flow impinges on mountain barriers. The Andes and the background flow are configured more like the Buzzi normal-mode experiment than the observations of Hsu (1987). Thus, the interaction of high-frequency disturbances with the Andes is better simulated by the normal modes in the presence of a mountain.

At 700 hPa (Fig. 9), the phase velocity is 17° of longitude per day and the wavelength is 60° of longitude. This shows that the high-frequency disturbances possess a higher phase velocity and a smaller wavelength than those noted in the unfiltered data. The mountain effects are clearly seen in this figure as indicated by the elongation of the center of correlation, the distortion in the isolines, and the appearance of a secondary maximum around 23°S, 64°W (Fig. 9d).

At 300 hPa (Fig. 10), the centers of maximum and minimum correlation over the Pacific Ocean propagate toward the east and are almost symmetric in the north–south direction. These features are similar to those of the normal modes over a plane surface. After crossing the continent, these centers develop a northwest–southeast horizontal tilt, which is also noted in the unfiltered data and is similar to what is seen in the Northern Hemisphere (Buzzi and Tosi 1989).

The analysis of correlation between 1000-hPa geopotential height at the base grid point 45°S, 70°W with all the grid points at 300 hPa (Fig. 11), shows that the disturbances exhibit a vertical inclination toward the west of about one-quarter wavelength, which seems to

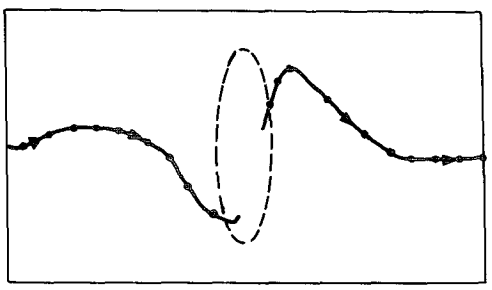

FIG. 13. Trajectory of the most unstable normal mode in the presence of a mountain range—adapted for the Southern Hemisphere. The mountain range is bi-Gaussian, with maximum height H_{max} = 2500 m. The broken line is the H_{max}/e contour. Dots mark position of cyclonic center at equally spaced times. Source: Buzzi et al. (1987).

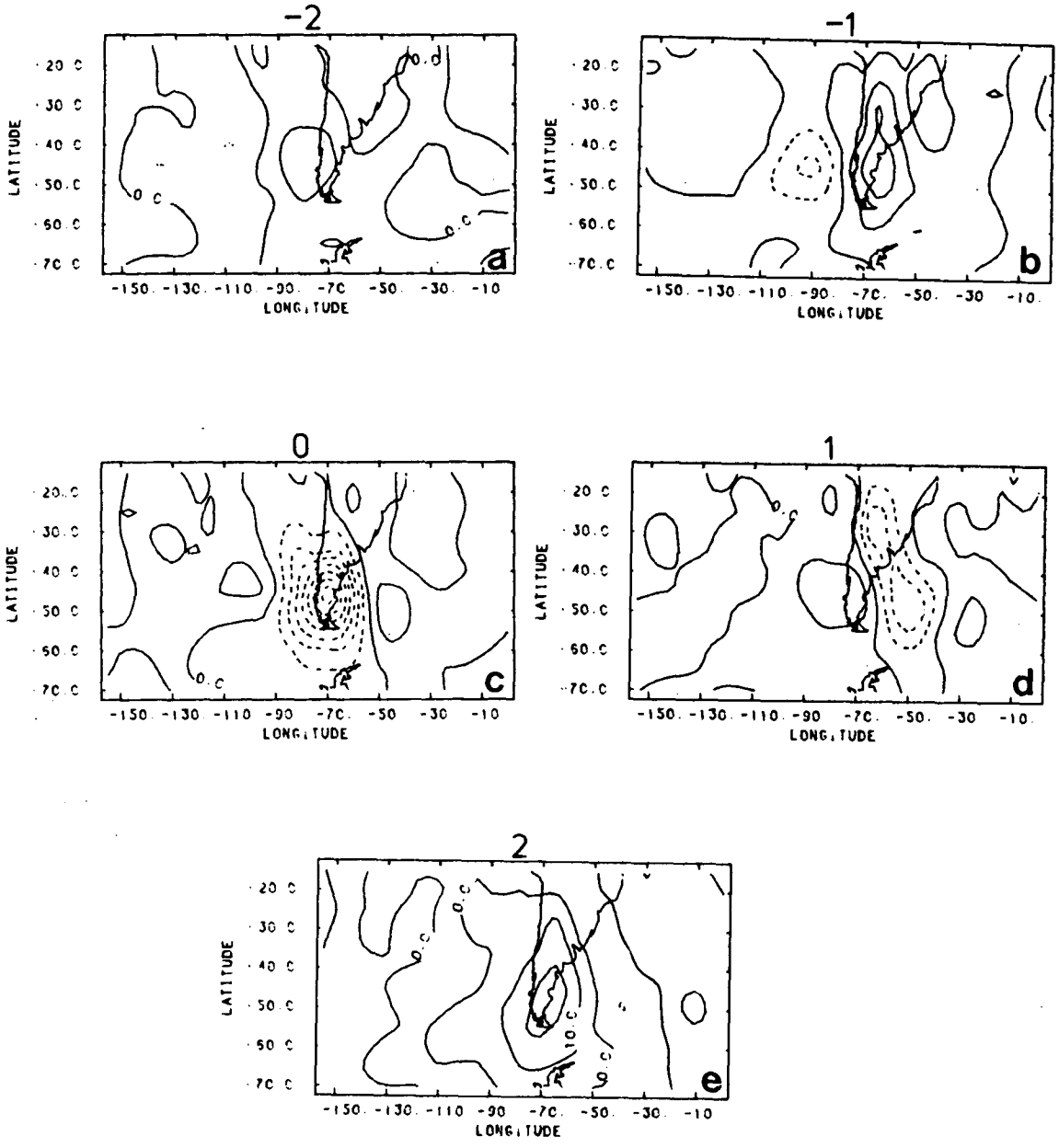

FIG. 14. Cyclonic system composite with high-pass-filtered 1000-hPa geopotential height data. The contour interval is 10 m: (a) 2 days earlier, (b) 1 day earlier, (c) at the same time, (d) 1 day later, and (e) 2 days later.

agree with the theoretical results on baroclinic waves (Charney 1947). The wave train at 300 hPa (Fig. 11) seems to possess a southwest–northeast orientation in the horizontal.

The trajectories of the centers of maximum correlation at 1000 hPa for the unfiltered and filtered data are shown in Fig. 12. In these two cases the trajectory of the disturbances is anticyclonic. For the unfiltered data, the flow on an f plane would provide a mountain-induced anticyclone that could explain the trajectory shown in Fig. 12. However, the anticyclonic turning of the trajectory for the filtered data is similar to that obtained by Buzzi et al. (1987) (Fig. 13) and is consistent with a Rossby wave. This Rossby wave could simply be associated with the β effect. But the distortions in the trajectory suggest that the Rossby wave could be a topographic Rossby wave in which the terrain slope provides an effective β.

The correlation maps presented here do not show differences between the negative and positive anomalies. However, climatological studies show that extratropical cyclones formed between 15° and 40°S prop-

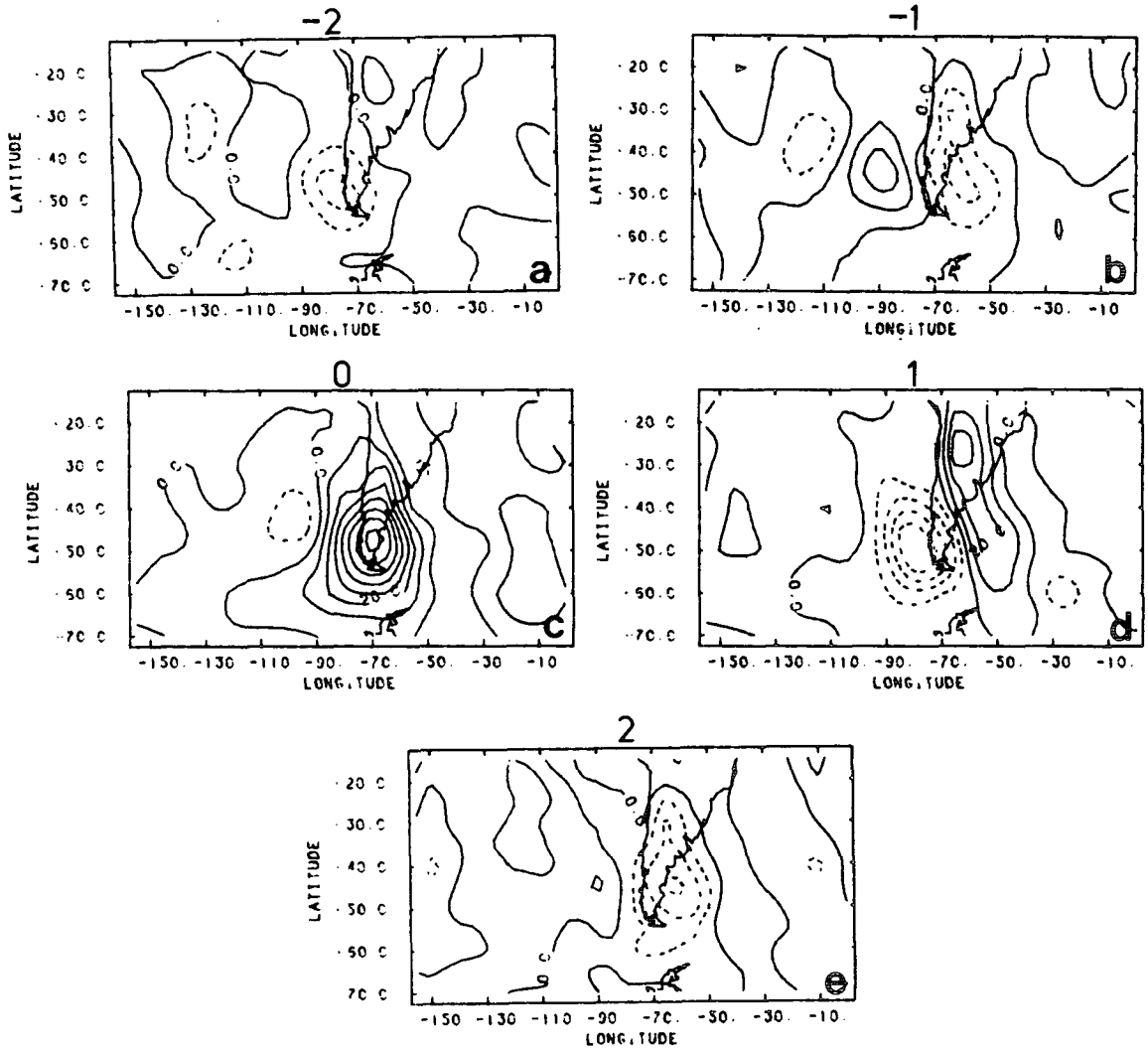

FIG. 15. Anticyclonic system composite with high-pass-filtered 1000-hPa geopotential height data. The contour interval is 10 m: (a) 2 days earlier, (b) 1 day earlier, (c) at the same time, (d) 1 day later, and (e) 2 days later.

agate toward the southeast (Gan 1992; Gan and Rao 1991) and anticyclones move toward the northeast (Lima 1991). Thus, it is necessary to construct composite maps separately for positive and negative anomalies. The criterion used to construct these maps is to select the filtered geopotential height data at 1000 hPa for the days when positive (negative) anomalies possess values exceeding or equal to two standard deviations above (below) the mean. Figure 14 shows the cyclone system composite at the 1000-hPa level for 61 cases of negative anomalies at the base point. It can be seen that there is a tendency for the disturbances to intensify over the eastern Pacific Ocean and over South America. It can also be noted that on days 0 and +1 (Figs. 14c,d) there exists a division of the negative anomalies—one center moves to the north of Argentina and the other center moves over the Atlantic Ocean. Other characteristics seen in the correlation maps such as the distortion of the isolines and the elongation of the anomalies on the lee side of the Andes are also observed.

Figure 15 shows the anticyclone system composite at 1000 hPa for 40 cases of positive anomalies at the base grid point. The characteristics of this figure are similar to those seen earlier at 1000 hPa in Fig. 7, including the northward displacement of the center of maximum geopotential height seen in Fig. 16. This indicates that the correlation analysis represents well the evolution of an anticyclone. Examination of surface synoptic charts for the South American region confirms this type of behavior for the transient anticyclones associated with a cold front.

The existence of a wave train of centers with a semicircular orientation can be seen in the cyclone system

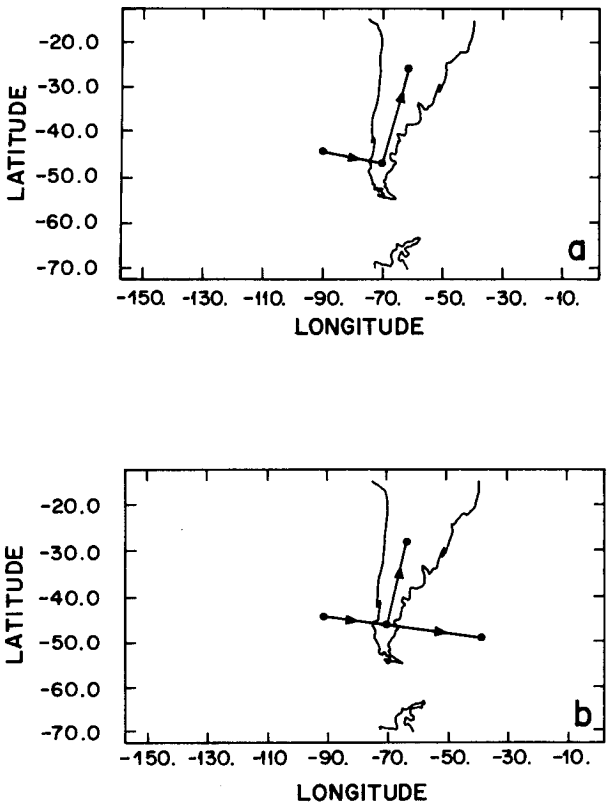

FIG. 16. Trajectory of anomaly at 1000 hPa: (a) positive; (b) negative. Temporal separation of the points is 24 h.

composite at 300 hPa (Fig. 17). This pattern intensifies from day −2 to day −1 (Figs. 17a,b). On day 0 (Fig. 17c), the centers of positive and negative anomalies over the continent and west coast both intensify. From day +1, this wave train moves in a zonal direction. It can be seen that the anomalies tend to intensify over the Pacific Ocean as they approach the west coast of South America. Comparing the positions of the centers of the anomalies at 300 hPa with those at 1000 hPa (Fig. 17 and Fig. 14), one can note that the anomalies incline toward the west with height by about one-quarter wavelength. This feature is also observed in the correlation maps. Figure 18 is similar to Fig. 17 except that it illustrates the anticyclone system composite. In this case the wave train does not possess a semicircular orientation, but the orientation is from northwest to southeast on day −2 (Fig. 18a), and on days 0 and +1 it changes to a zonal direction. Another point that has to be stressed here is that the 1000- and 300-hPa-level anomalies grow practically at the same time, although they weaken first in the lower levels.

4. Summary and discussion

The analysis of cross correlation of geopotential height is shown to be an efficient tool in studying the spatial and temporal characteristics of transient disturbances and their interactions with the mountain (Hsu 1987; Wallace et al. 1988). This method is successful because the disturbances maintain a spatial coherence longer than their wavelength and a temporal coherence larger than their period (Buzzi et al. 1989).

The analysis of correlation of unfiltered geopotential height, using a base grid point to the east of the Andes, shows a wave pattern that represents well the pattern of low-frequency anomalies. This wave pattern propagates eastward and shows orographic effects after crossing the Andes, such as the distortions in the isolines of correlation and elongation of the center of maximum correlation. These distortions might also be due to the thermal contrast between the ocean and the continent on the west coast. However, since these distortions do not appear on the east coast and since they are clearly seen in the normal modes in the presence of mountains (Fig. 8), it can be concluded that these distortions are due to the presence of mountains.

Frederiksen and Frederiksen (1991) studied the role of orographic forcing in a spherical barotropic quasi-geostrophic instability model. Their results show that topography can promote the growth of perturbations either through a form drag mechanism, which modifies the globally averaged angular momentum of the basic state, or through its action as a catalyst that can initiate wave–wave interactions between the basic state and the disturbance while leaving the globally averaged angular momentum unchanged.

Using a primitive equations model in sigma coordinates, Bratseth and Breivik (1988) developed a theory for lee cyclogenesis. According to them, when a baroclinic zone passes over a high mountain, the thermal field will be deformed and some kind of development will take place. They also suggested that the degree of deformation and cyclogenesis depends heavily on the possibility of resonant interaction between the orographic forcing and the baroclinic waves. Thus, the distortions in the isolines of correlation noted in Figs. 2, 3, 7, 9, 14, and 15 might be associated with the resonant interaction between the topographic Rossby wave and baroclinicity.

The elongation of the center of maximum correlation and a westward inclination with height observed in Figs. 2 and 5 are due to the interaction of the baroclinic disturbance with the stationary wave generated by the mountains. It has been shown by several authors (Longuet-Higgins 1968; Rhines 1969; Johnson 1984) that the first eigenmode of a topographic Rossby wave exhibits a spatial scale comparable to that of the topographic features. Unlike the higher modes, these modes are rather insensitive to the fine structure of the topographic features. Since the lateral scale noted in the isolines of correlation maps seems to be comparable to the topographic features, the waves noted in the correlation field could be interpreted as smooth topographic Rossby waves.

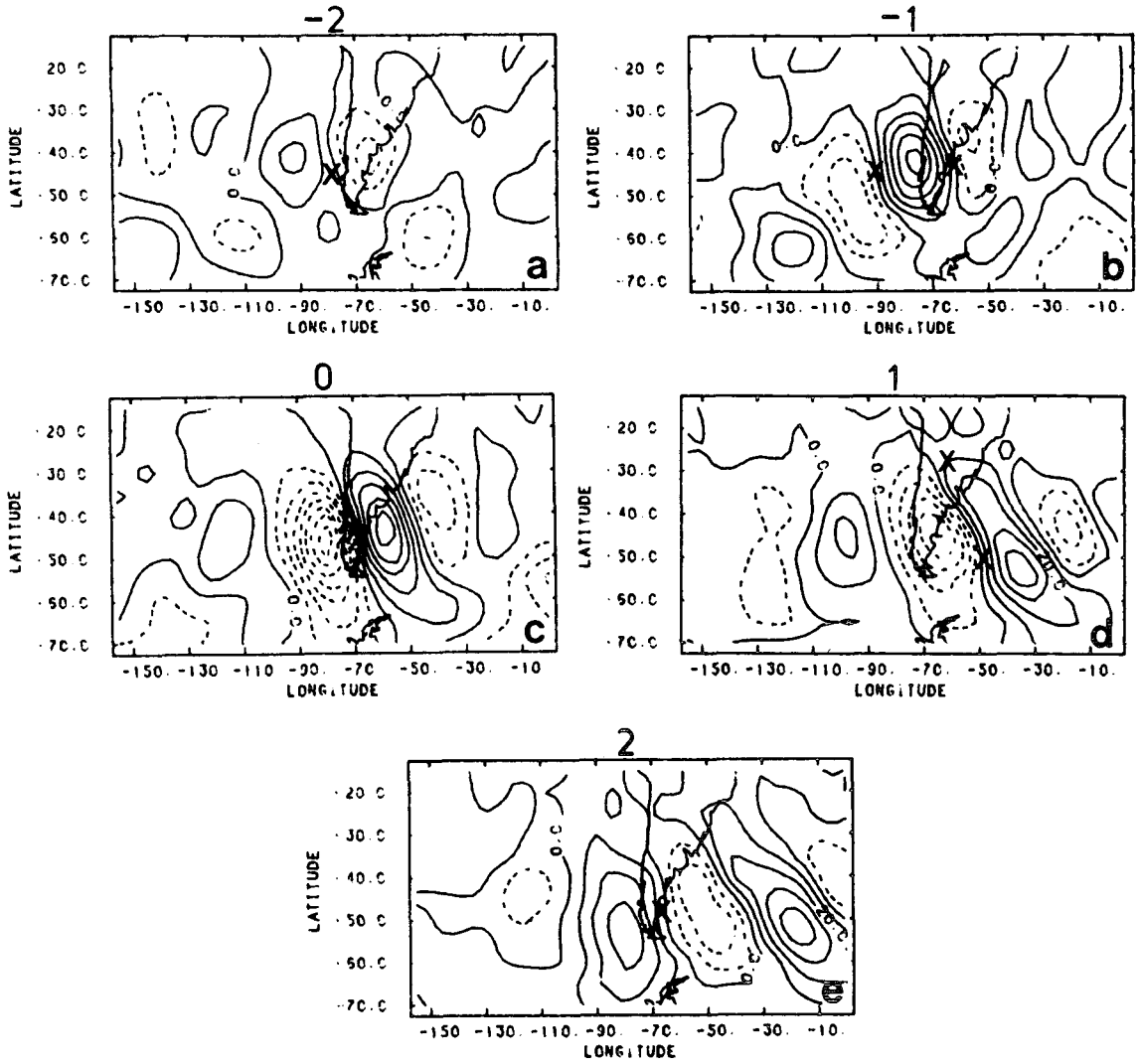

FIG. 17. Cyclonic system composite with high-pass-filtered 300-hPa geopotential height data. The contour interval is 10 m: (a) 2 days earlier, (b) 1 day earlier, (c) at the same time, (d) 1 day later, and (e) 2 days later. The "X" represents the respective minimum or maximum center at 1000 hPa.

The wave pattern observed in the correlation of unfiltered geopotential height data shows a slight inclination to the west in the vertical over the Pacific Ocean and a strong inclination to the west in the vertical over the eastern part of the Andes indicating the effect of baroclinicity. This increase in baroclinicity results in baroclinic development as shown in a linear quasigeostrophic model including a mountain range aligned in the north–south direction (Buzzi et al. 1987).

The same statistical analysis performed for high-pass-filtered data for the base grid point 45°S, 70°W revealed the existence of a wave pattern that propagates eastward with a spatial scale smaller than that noted for unfiltered data and shows an inclination of about one-quarter wavelength between the 1000- and 300-hPa levels. The centers of correlation show distortions in the isolines of correlation, elongation of the center of maximum and minimum correlation, and a displacement of the center of maximum correlation toward the north. This horizontal structure is similar to the most unstable normal mode in a two-layer, quasigeostrophic, β-plane, linear model with a mountain range placed in a north–south direction, obtained by Buzzi et al. (1987). These results confirm the presence of cyclogenesis on the lee side of the Andes. Although some of the results presented here are consistent with the depictions of the fastest-growing normal modes, present theories do not seem to adequately describe lee cyclogenesis. This is particularly so in the Alpine cyclogenesis (Tafferner and Egger 1990).

The composite charts of cyclone and anticyclone system showed that the positive and negative anomalies

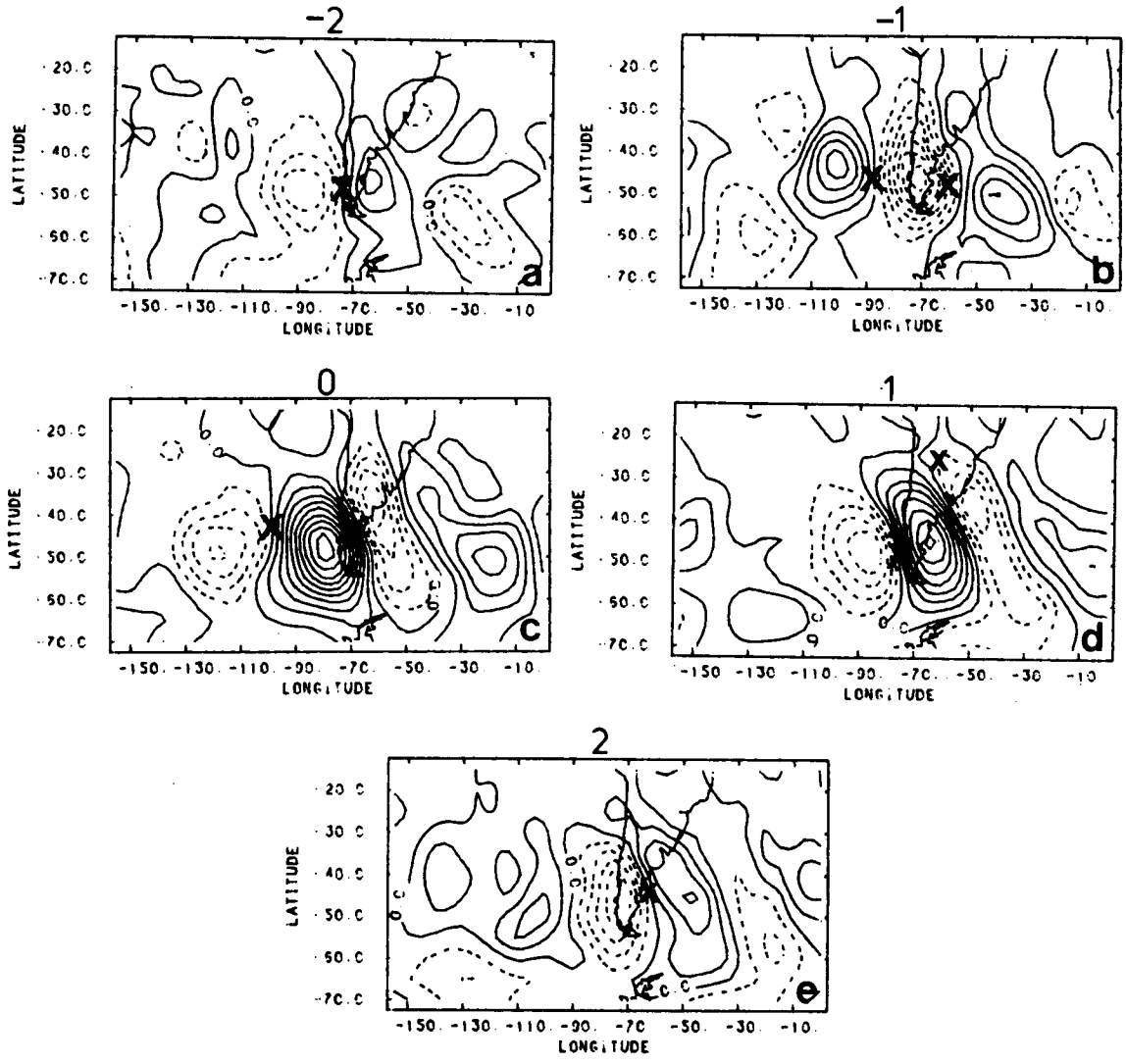

FIG. 18. Anticyclonic system composite with high-pass-filtered 300-hPa geopotential height data. The contour interval is 10 m: (a) 2 days earlier, (b) 1 day earlier, (c) at the same time, (d) 1 day later, and (e) 2 days later. The "X" represents the respective minimum or maximum center at 1000 hPa.

possess the same trajectories, although Gan and Rao (1991) noted that extratropical cyclones move toward the southeast, and Lima (1991) noted that anticyclones move toward the northeast. Wallace et al. (1988) observed that the trajectories of positive and negative anomalies in the Northern Hemisphere are similar and they generally tend to travel along the waveguides.

The positive and negative anomalies also show a tendency to intensify over the eastern Pacific Ocean near South America. The intensification of the anomaly occurs over all the pressure levels at the same time, but the decay of the anomaly occurs first at lower levels.

Acknowledgments. The present work is taken from the Ph.D. dissertation of the first author. We are grateful to Prof. J. M. Wallace of the University of Washington, Seattle, for going through the manuscript and offering valuable comments. Thanks are due to official reviewers and to the editor Dr. Daniel Keyser for suggesting further improvements to the text. Thanks are also due to Dr. M. R. Stevenson for critically going through the manuscript.

REFERENCES

Bratseth, A. B., and B. A. Breivik, 1988: A numerical study of a lee cyclogenesis theory. *Palmén Memorial Symp. on Extratropical Cyclones,* Helsinki, Finland, Amer. Meteor. Soc., 269–272.

Buzzi, A., and S. Tibaldi, 1978: Cyclogenesis in the lee of the Alps: A case study. *Quart. J. Roy. Meteor. Soc.,* **104,** 271–287.

——, and E. Tosi, 1989: Statistical behaviors of transient eddies near mountains and implications for theories of lee cyclogenesis. *J. Atmos. Sci.,* **46,** 1233–1249.

——, A. Speranza, S. Tibaldi, and E. Tosi, 1987: A unified theory of orographic influences upon cyclogenesis. *Meteor. Atmos. Phys.*, **36,** 91–107.

——, P. Malguzzi, and A. Trevisan, 1990: The statistical properties of the interaction of high-frequency eddies with mountains in a two-layer model. *Tellus,* **42A,** 28–40.

Charney, J. G., 1947: The dynamics of long waves in a baroclinic westerly current. *J. Meteor.*, **4,** 135–162.

Egger, J., 1972: Numerical experiments on cyclogenesis in the Gulf of Genoa. *Phys. Atmos.*, **45,** 320–346.

——, 1974: Numerical experiments on lee cyclogenesis. *Mon. Wea. Rev.*, **102,** 847–860.

Eliassen, A., and E. Palm, 1961: On the transfer of energy in stationary mountain waves. *Geofys. Publ.*, **22,** 1–23.

Frederiksen, C. S., and J. S. Frederiksen, 1991: Flow over topography and instability on a sphere. *J. Atmos. Sci.*, **48,** 2411–2425.

Gan, M. A., 1992: Ciclogêneses e ciclones sobre a América do Sul. (Cyclogenesis and cyclones over South America.) Ph.D. dissertation, Instituto de Pesquisas Espaciais—São Paulo, Brazil.

——, and V. B. Rao, 1991: Surface cyclogenesis over South America. *Mon. Wea. Rev.*, **119,** 1293–1302.

Hayes, J. L., R. T. Williams, and M. A. Rennick, 1987: Lee cyclogenesis. Part I: Analytic studies. *J. Atmos. Sci.*, **44,** 432–442.

Hsu, H. H., 1987: Propagation of low-level circulation features in the vicinity of mountain ranges. *Mon. Wea. Rev.*, **115,** 1864–1892.

Johnson, E. R., 1984: Starting flow for an obstacle moving transversely in a rapidly rotating fluid. *J. Fluid Mech.*, **149,** 71–88.

Lau, N. C., and K. M. Lau, 1984: The structure and energetics of midlatitude disturbances accompanying cold-air outbreaks over east Asia. *Mon. Wea. Rev.*, **112,** 1309–1327.

Lima, L. C. E., 1991: An observational study of formation and trajectories of extratropical anticyclones over the South American continent. M.S. thesis, Instituto de Pesquisas Espaciais—São Paulo, Brazil.

Longuet-Higgins, M. S., 1968: On the trapping of waves along a discontinuity of depth in a rotating ocean. *J. Fluid Mech.*, **31,** 417–434.

McGinley, J. A., 1982: A diagnosis of Alpine lee cyclogenesis. *Mon. Wea. Rev.*, **110,** 1271–1287.

——, and M. Zupanski, 1990: Numerical analysis of the influence of jets, fronts and mountains on alpine lee cyclogenesis: More cases from the Alpex sop. *Meteor. Atmos. Phys.*, **43,** 7–20.

Palmén, E., and C. M. Newton, 1969: *Atmospheric Circulation Systems.* Academic Press, 603 pp.

Pichler, H., and R. Steinacker, 1987: On the synoptics and dynamics of orographically induced cyclones in the Mediterranean. *Meteor. Atmos. Phys.*, **36,** 108–117.

Randel, W. J., and J. L. Stanford, 1985a: An observational study of medium-scale wave dynamics in the Southern Hemisphere summer. Part I: Wave structure and energetics. *J. Atmos. Sci.*, **42,** 1172–1188.

——, and ——, 1985b: An observational study of medium-scale wave dynamics in the Southern Hemisphere summer. Part II: Stationary-transient wave interference. *J. Atmos. Sci.*, **42,** 1189–1197.

——, and ——, 1985c: The observational life cycle of a baroclinic instability. *J. Atmos. Sci.*, **42,** 1364–1373.

Rhines, P. B., 1969: Slow oscillations in an ocean of varying depth. Part I: Abrupt topography. *J. Fluid Mech.*, **37,** 161–189.

Satyamurty, P., R. P. Santos, and M. A. M. Lemes, 1980: On the stationary trough generated by the Andes. *Mon. Wea. Rev.*, **108,** 510–519.

Speranza, A., A. Buzzi, A. Trevisan, and P. Malguzzi, 1985: A theory of deep cyclogenesis in the lee of the Alps: Modifications of baroclinic instability by localized topography. *J. Atmos. Sci.*, **42,** 1521–1535.

Tafferner, A., and J. Egger, 1990: Test of theories of lee cyclogenesis: Alpex cases. *J. Atmos. Sci.*, **47,** 2417–2428.

Wallace, J. M., 1986: Observations of orographic influences upon large scale atmospheric motions. *Seminar/Workshop of Observation, Theory and Modelling of Orographic Effects,* Reading, United Kingdom, European Centre for Medium-Range Weather Forecasts, 23–49.

——, G. H. Lim, and M. Blackmon, 1988: Relationship between cyclone tracks, anticyclone tracks, and baroclinic waveguides. *J. Atmos. Sci.*, **45,** 439–462.

WMO, 1980: Orographic effects in planetary flows. GARP Publications No. 23, 450 pp.